# Electrochemical characterization of shape-controlled Pt nanoparticles in different supporting electrolytes

*Francisco J. Vidal-Iglesias, Rosa M. Arán-Ais, José Solla-Gullón, Enrique Herrero*, Juan M. Feliu**

Instituto de Electroquímica, Universidad de Alicante, Apartado 99, 03080 Alicante (Spain)

*CORRESPONDING AUTHOR E-MAIL ADDRESS: herrero@ua.es; juan.feliu@ua.es

**RECEIVED DATE**

ABSTRACT.

The voltammetric profile of preferentially shaped platinum nanoparticles has been used to analyze of the different sites present on the surface. This analysis has been made, for the first time, in NaOH solutions and revisited in sulfuric and perchloric acid media. The comparison with the voltammetric profiles of the model surfaces, i.e., single crystal electrodes, allows assigning the different signals appearing in the voltammograms of the nanoparticle to specific sites on the surface. A good correlation between the shape of the nanoparticle determined by TEM and the voltammetric profile is obtained. For the nanoparticles characterized in alkaline media, the adsorbed species on the surface has been characterized and three major regions can be identified. Below 0.2 V, the major contribution is due to hydrogen adsorption whereas above 0.6 V, adsorbed OH is the main species on the surface. In between both values, the signals are due to competitive adsorption/desorption process of OH/H. New criteria for determining the active area in NaOH solutions has been proposed. In this medium, the total charge density measured between 0.06 and 0.90V stands for 390 μC $cm^{-2}$. The areas measured are in perfect agreement with those measured in acid media. Once the nanoparticles

have been characterized, the behavior of the nanoparticles towards CO oxidation has been analyzed. It has been found that the nanoparticle edges are key sites in the oxidation of CO.

KEYWORDS. Platinum, nanoparticles characterization, alkaline media, CO oxidation.

## Introduction

It is well-established that most of the electrocatalytic reactions of interest are structure sensitive. This effect has been well documented by using single crystal electrodes. In some cases, such as hydrogen oxidation or oxygen reduction, the reactivity of the single crystal electrodes is similar, albeit some reactivity differences (measured current density at constant potential) can be observed.[1-3] These differences are more significant for the oxidation of potential organic fuels or for nitrogen containing compounds.[4, 5] In some particular cases, the reaction only takes place on a particular type of surface site.

For practical purposes, nanoparticle electrocatalysts dispersed on a suitable support are used. As the reaction takes place on the surface sites, the surface structure of the nanoparticle will strongly control their reactivity. In the last years, the synthesis of shape-controlled Pt nanoparticles has been widely explored with the main objective of obtaining more efficient catalysts.[6-9] Thus, it has been clearly shown that the reactivity and selectivity of the Pt nanoparticles can be modulated by controlling the morphology, because the surface of the nanoparticles may contain very different reactive surface sites depending on their shape.[7, 10] In addition, these shape controlled nanoparticles are ideal to understand the reactivity of practical electrodes since they provide the missing link with the model surfaces, i.e., the single crystal electrodes. However, the preparation of shape-controlled Pt nanoparticles requires, in most of the cases, the use of surface-stabilizing agents. Consequently, once the nanoparticles are synthesized, these stabilizing agents must be completely removed from the surface of the nanoparticles because, as previously stated, chemical or electrochemical reactions can be only understood on “clean” surfaces. Obtaining reproducible measurements requires the comparison between data on clean surfaces, because “contaminated” surfaces have unknown

composition. Reproducibility is a key factor in Science, that is, progress in the understanding of surface reactivity requires standard procedures to be fulfilled on the different laboratories. However, one question arises from this requirement: how should surface cleaning be evaluated? Fortunately, after more than 30 years of working with Pt in electrocatalysis, the level of cleanliness of the Pt surfaces can be readily evaluated by simply visualizing the so-called hydrogen adsorption desorption region.[11] Thus, the peak position, definition (sharpness) and the reversibility of the adsorption states in the so-called hydrogen and anion adsorption region can be employed as probes to estimate the surface cleanliness of the Pt nanoparticles, an imperative pre-requisite for a correct surface characterization and further electrocatalytic evaluation. Consequently, the criteria developed for validating single crystal experiments should be also considered when the reactivity of nanoparticles is examined, which would allow gaining the comprehensive understanding of their intrinsic catalytic or electrocatalytic properties.

Interestingly, this hydrogen and anion adsorption region can also be used as probe reactions to define the properties of the surface. Two main reasons justify the use of this region for this purpose. First, the overall adsorption charge is directly proportional to the amount of surface atoms and thus can be used to calculate the real surface area. Second, it is well-established that the orientation, the type of ordered domains, and the density of step sites of a Pt single crystal plane including basal, stepped and kinked surfaces could be readily characterized by using its voltammogram in the so-called hydrogen adsorption/desorption region.[12-16] Consequently, in case of the shape-controlled Pt nanoparticles, the distribution of the charge among the different voltammetric peaks gives a first estimation of the presence of the different surface sites on the whole surface.[12, 17] Additionally, the characteristic response of the surface sites present at the nanoparticles can be analyzed by simply comparison with model single crystal stepped surface electrodes, which consist of a regular succession of terraces with a given symmetry separated by monoatomic steps with a different, but controlled, symmetry. By changing the terrace width and the symmetry of the step, the contributions of the different domains can be analyzed and linked to the results of the real surfaces. An additional advantage is that all these measurements may be performed in solution, i.e. the environment in which electrochemical reactions occur.

In this paper we report and discuss the electrochemical response of some representative shape-controlled Pt nanoparticles in the so-called hydrogen adsorption/desorption region for different electrolytes. This analysis is made, for the first time, in NaOH solution and revisited for $H_2SO_4$ and $HClO_4$ solutions. The results obtained will be correlated with those coming from model single crystal Pt surfaces. Interestingly, a new criterion for determining the active surface area in NaOH is presented based on the analysis of the electrochemical response of the different Pt basal planes as well as some stepped and kink surfaces obtained in the same experimental conditions as those employed in case of the different nanoparticles as well as on the comparison with the active surface area of the nanoparticles determined in the other supporting electrolytes ($H_2SO_4$ and $HClO_4$). A correct determination of the active surface area is a question of paramount importance in Electrocatalyis because allows properly measuring the intrinsic electrocatalytic properties of the system under study. Additionally, in this alkaline media, we also report new insights into the CO stripping oxidation on the different shape controlled Pt nanoparticles. These new results will be discussed in terms of CO electrooxidation on well-defined stepped Pt single crystals which has been recently studied in detail. [18-22]

## Experimental

### Synthesis and cleaning of the Pt nanoparticles

In this work, four types of Pt nanoparticles were prepared. Comprehensive experimental details on the synthesis are given in the supporting material. In brief, Pt nanoparticles with preferential spherical shape ($PtNP_{sphe}$) were synthesized by reducing $H_2PtCl_6$ with sodium borohydride using a water-in-oil (w/o) microemulsion.[23-26] The other three types of nanoparticles (with preferential cubic shape ($PtNP_{cubic}$), with preferential octahedral tetrahedral shape ($PtNP_{tetra}$) and with preferential octahedral and tetrahedral truncated shape ($PtNP_{trunc}$)) were synthesized with a colloidal method using sodium polyacrylate (PA, Mw = 2100) as capping agent, $K_2PtCl_4$ or $H_2PtCl_6$ as metallic precursor, and $H_2$ as reducing agent.[25, 27, 28]

### Cleaning process for the shape-controlled Pt nanoparticles

After complete reduction (12-14 hours), the shape-controlled Pt NPs were cleaned with strong basic aqueous solution followed by several water washes to finally achieve a water suspension with clean Pt nanoparticles. For the present experimental conditions (100 ml of solution), two NaOH pellets (≈ 0.2 g) are added to the colloidal suspension containing the shape-controlled Pt nanoparticles. Once NaOH is dissolved, the sample is left to stand until complete precipitation. After solvent removal, the nanoparticles were washed 3-4 times with ultra-pure water. The previously described cleaning procedures should be considered exclusively valid for the current synthetic methodologies and should not be taken as a general cleaning method. For instance, we have tried to employ the same cleaning methodology for shape-controlled Pt nanoparticles synthesized with PVP, which is one of the most widely employed stabilizing agents, with negative results.

Characterization of Pt nanoparticles by TEM

Transmission Electron Microscopy (TEM) and High Resolution Transmission Electron Microscopy (HRTEM) have been employed to investigate the shape of the nanoparticles at the atomic scale. TEM experiments were performed with a JEOL, JEM 2010 microscope working at 200 kV whereas HRTEM experiments have been carried out on a JEOL 3010 microscope (LaB6, Cs=1.1 mm) operated at 300 kV, providing a point-to-point resolution of 0.19 nm. The sample was obtained by placing a drop of the dispersed solution onto a Formvar-covered copper grid and evaporating it in air at room temperature. For each sample, usually more than 200 particles from different parts of the grid were used to estimate the mean diameter and size distribution of the nanoparticles. Despite the micrographs only provide a 2D projection of these particles, they clearly evidence that the nanoparticles crystallize with different shapes.

Platinum single crystal electrodes

Platinum single crystals were oriented, cut and polished from small single crystal beads (~2.5 mm diameter) by the procedure described previously.[29] The electrodes were flame-annealed and cooled down in a $H_2$ + Ar atmosphere in the usual way.[30] It has been shown that this treatment leads to well-defined surfaces.[31] A single crystal platinum bead obtained by fusion of a Pt wire was used as a polycrystalline surface having uniform distribution of all surface sites (Pt poly). A detailed description of the single crystal surfaces is given in the supporting information (table S1).

Electrochemical characterization

The electrochemical characterization of the samples, both single crystal surfaces and Pt nanoparticles, was performed in a three-electrode electrochemical cell. The electrode potential was controlled using a PGSTAT30 AUTOLAB system. The counter electrode was a gold wire. Potentials were measured against a reversible hydrogen electrode (RHE) connected to the cell through a Luggin capillary. For the Pt nanoparticles, a droplet ranging from 1 to 3 μL of the solution containing the nanoparticles was deposited on a hemispherical polycrystalline gold substrate and dried under an Ar atmosphere. Before each experiment, the gold collector was mechanically polished with alumina and rinsed with ultra-pure water to eliminate the nanoparticles from previous experiments. In order to perform the adsorbed CO oxidation experiments, CO(g) was bubbled through the electrolyte at an admission potential of 0.05 V until the complete blockage of the surface was reached, which was monitored by cycling the electrode between 0.05 and 0.35 V. After that, CO was removed from the solution by bubbling Ar for at least 20 min. CO-stripping voltammograms were registered at 20 mV $s^{-1}$ in order to oxidize the CO molecules adsorbed on the surface in a single sweep. The supporting electrolytes, 0.5 M $H_2SO_4$ and 0.1 M $HClO_4$, were prepared from suprapur quality (Merck) and 0.1 M NaOH solutions from p.a. quality (Merck) NaOH pellets. Solutions were prepared using Millipore MilliQ water. Oxygen was eliminated by bubbling Ar (Air Liquide N50) for 20 min.

The determination of the active surface area of the Pt nanoparticles is a question of paramount importance in Electrocatalyis because allows properly determining the intrinsic electrocatalytic properties of the system under study. In the present work, the active surface area of the different Pt

nanoparticles was determined in $H_2SO_4$ and in $HClO_4$ by the charge involved in the so-called hydrogen UPD region assuming 230 μC $cm^{-2}$ and 200 μC $cm^{-2}$ respectively, for the total charge after the subtraction of the double layer charging contribution as previously discussed.[10] However, in case of the alkaline medium, the determination of the active surface area is not straightforward and will be studied in more detail in the present manuscript.

**Results**

Voltammetric characterization of the nanoparticles

$PtNP_{sphe}$, $PtNP_{cubic}$, $PtNP_{tetra}$ and $PtNP_{trunc}$ nanoparticles with a particle size of 4.5 ± 0.8 nm, 8.2 ± 1.6 nm, 8.5 ± 1.4 nm and 9.7 ± 1.6 nm respectively, were successfully obtained after synthetic procedures (see figs. S1-S3 for some representative TEM and HRTEM images of the Pt nanoparticles as well as their particle size histograms). In terms of surface structure, these samples can be assigned to polyoriented, (100), (111), and (111)-(100) preferentially oriented Pt nanoparticles, respectively.

Fig. 1 shows the characteristic voltammetric profiles of the different Pt nanoparticles in 0.5 M $H_2SO_4$, after effective cleaning of their surfaces. The sharpness, good definition and the symmetry of the adsorption states in all samples are clear evidences of the effective surface cleanliness. The analysis of the characteristic voltammetric features obtained in this media was already discussed in detail in a previous contribution.[24] In summary, the main voltammetric features are i) the peak at 0.125 V, which is related to (110)-type sites, ii) the peak at 0.27 V, with contains two contributions from (100) step sites on (111) terraces and the sites close to the steps on the (100) terraces, iii) the signals 0.35-0.37 V attributed to (100) bidimensional terraces and iv) the signals at 0.5 V, related to the bidimensionally ordered (111) terraces. All these voltammetric profiles perfectly correlate with those obtained with Pt single crystal electrodes (Fig. S4). In this way, this simple electrochemical experiment can give us a first estimation of the presence of the different surface sites on the whole surface as well as evidence of the surface cleanliness. Interestingly, all these states are observed in all Pt nanoparticles but in a different extent, which reflects their specific surface structure

composition, in agreement with that suggested by the TEM measurements. Additionally, surface probes sensitive to specific sites such as Bi,[24, 32, 33] Ge[24, 34, 35] or Te[24, 36] adsorption and the deconvolution of the voltammetric profiles[24] allow quantifying the relative amount of sites present on the surface of the nanoparticle (see table S2). These values are in very good agreement with the preferential shape determined from the TEM images. Thus, the voltammetric profile of $PtNP_{cubic}$ exhibits the largest contributions at 0.35-0.37 V assigned to the (100) ordered domains, whereas the (111) nanoparticles have the highest currents in the region corresponding to the (111) domains. In addition, it is worth noting that despite of the size and shape dispersion of the samples, the voltammetric profile of each particular sample which reflects their surface structure, it is always the same for different aliquots of the sample in independent experiments. Consequently, their voltammetric profile can be used as fingerprint of their specific surface structure.

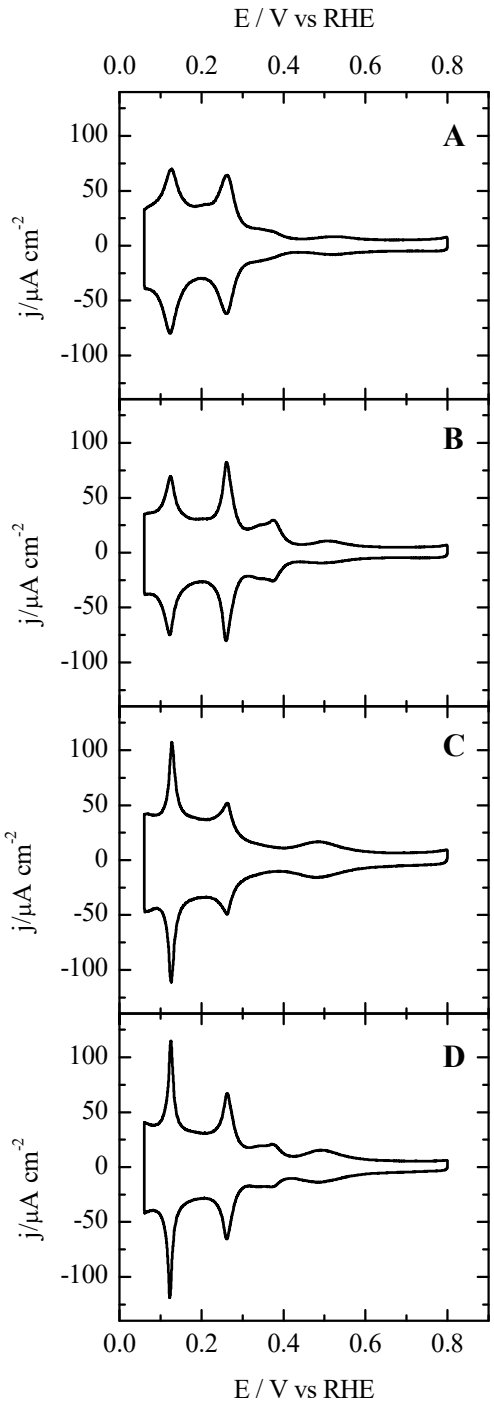


**Figure 1.** Voltammograms corresponding to (A) $PtNP_{sphe}$, (B) $PtNP_{cubic}$ (C) $PtNP_{tetra}$ and (D) $PtNP_{trunc}$ in 0.5 M $H_2SO_4$. Scan rate 50 mV $s^{-1}$.

Switching to $HClO_4$, and although it is known that the adsorption desorption peaks are not as well resolved in this electrolyte as in sulfuric acid, different voltammetric profiles can be also obtained in this media from distinct shape of the nanoparticles. In addition, it should be highlighted

that the absence of specific anion adsorption causes that the different adsorption states spread in a wider potential range, that is, the peaks become wider. This broader profile makes more difficult to identify by simple inspection that the nanoparticle surfaces are clean, in comparison to the data in sulfuric acid. Figure 2 shows the voltammograms obtained for the different Pt nanoparticles. By comparison with those obtained with Pt single crystal electrodes, figure 3, it is possible to identify the main voltammetric features in this electrolyte. In detail, the contributions in the range between 0.3-0.5 V can be clearly related to the presence of (100) sites due to OH adsorption on the (100) well-ordered domains as proposed for the single crystal electrodes with this orientation.[37, 38] Thus, the voltammograms of the $PtNP_{cubic}$, and also that of the $PtNP_{trunc}$, although that in a lesser extent, show a significant broad contribution in this region in agreement with their preferential surface orientation as well as the results obtained in sulfuric media. This contribution is absent in the $PtNP_{tetra}$, which have a very low amount of well ordered (100) domains. On the other hand, the contributions in the range between 0.09-0.22 V can be attributed to (110) sites. Interestingly, a clear splitting in at least three different contributions, not observed in sulfuric acid, can be observed. Similar behavior has been observed in the voltammetry of Pt(110) single crystal electrodes and its vicinal surfaces in perchloric acid and points out the complexity of this adsorption state, which is the least studied among the platinum single crystal basal planes.[39-41] Finally, in this solution, the (111) bidimensional states cannot be identified, as they are shifted towards high potentials and overlap with oxygenated species adsorption at (100) and (110) sites, making difficult its identification because does not show prominent peaks below 0.35 V. As happens in sulfuric acid, (111) sites give a flat contribution on the 0.06-0.30 V region, which cannot be distinguished from those coming from the double layer charging processes.

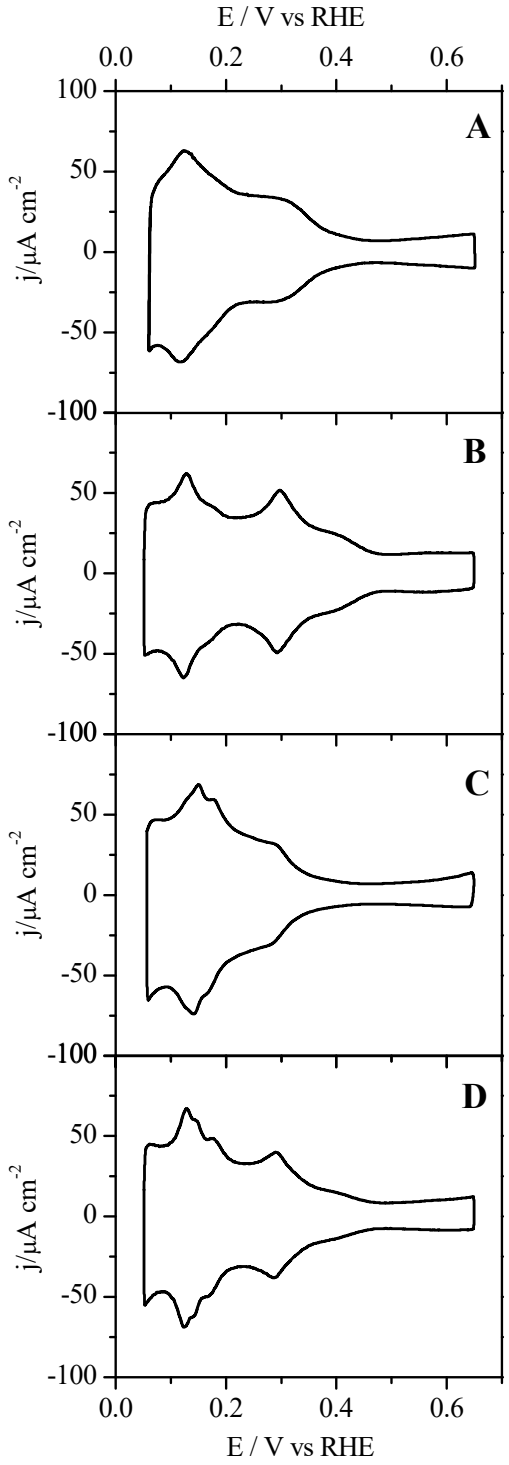


**Figure 2.** Voltammograms corresponding to (A) $PtNP_{sphe}$, (B) $PtNP_{cubic}$ (C) $PtNP_{tetra}$ and (D) $PtNP_{trunc}$ in 0.1 M $HClO_4$. Scan rate 50 mV $s^{-1}$.

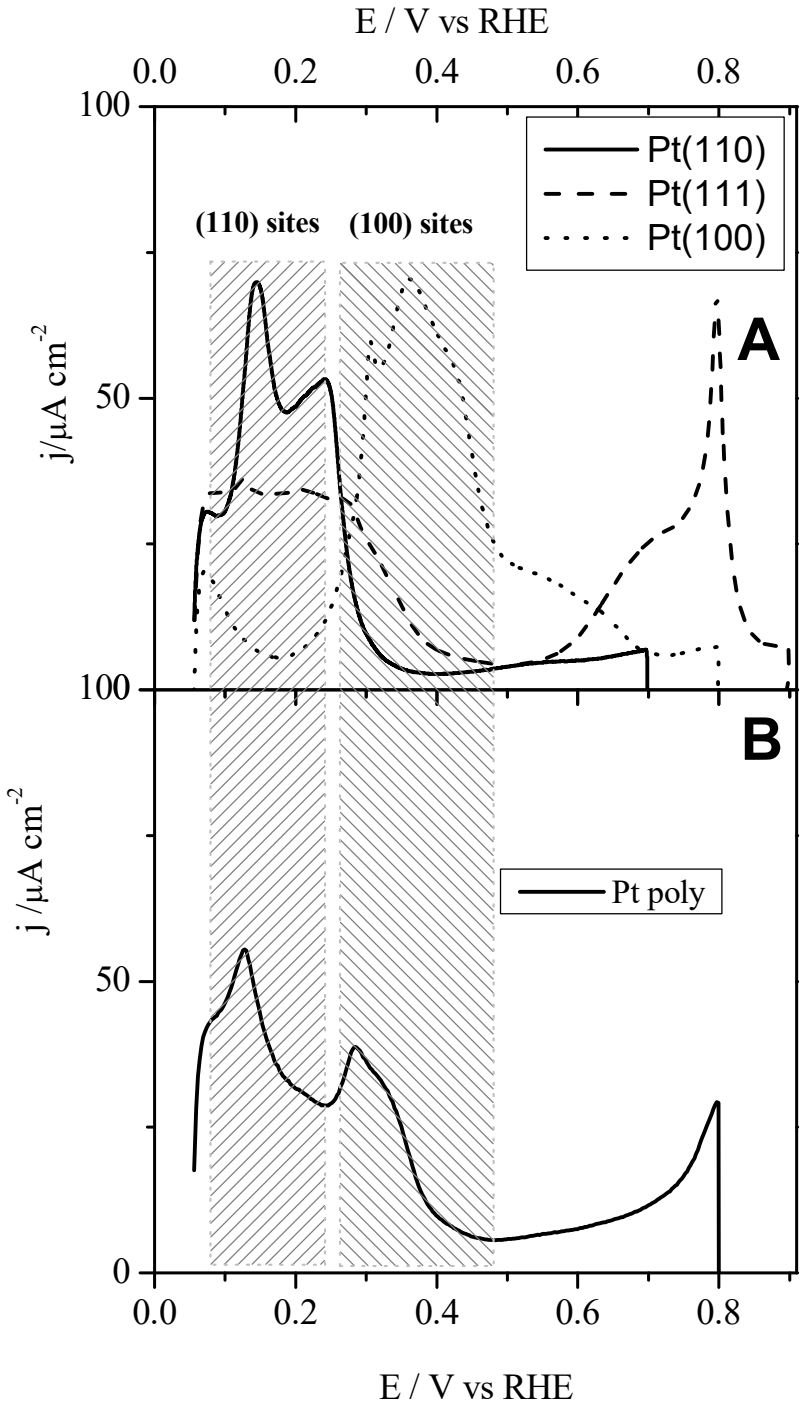


**Figure 3**. Voltammetric profiles of the Pt basal planes (A) to compare their site distribution with those obtained with a polyoriented platinum electrode (B) in 0.1 M $HClO_4$. Scan rate: 50 mV $s^{-1}$.

Finally, figure 4 shows the characteristic voltammetric profiles of the different shape controlled Pt nanoparticles in alkaline media (0.1 M NaOH). In these voltammetric profiles, the contribution from the gold support has been subtracted in all cases, to obtain the "net" voltammetric profile of the

nanoparticles. This contribution is important in alkaline media due to the higher amount of OH adsorption on gold in the range between 0.5-0.9 V. Figure 5 shows the black voltammograms of the gold support as well as the black CV of one of the samples and the resulting CV after subtraction. As previously stated, the major changes occur in the range between 0.5-0.9 V remaining the contributions in the lower potential range almost invariable.

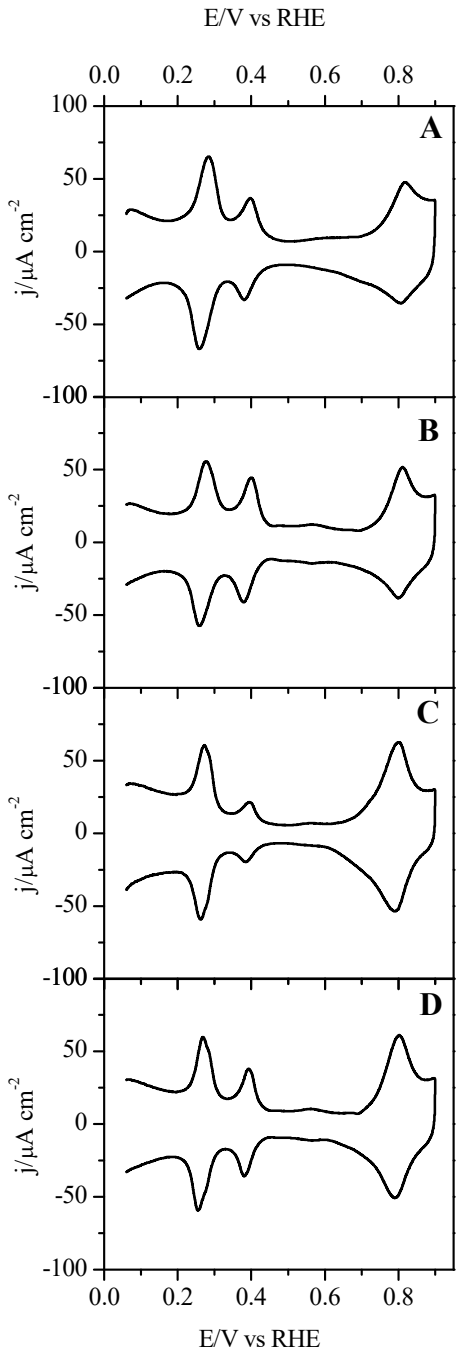


**Figure 4.** Voltammograms corresponding to (A) $PtNP_{sphe}$, (B) $PtNP_{cubic}$ (C) $PtNP_{tetra}$ and (D) $PtNP_{trunc}$ in 0.1 M NaOH. Scan rate 50 mV $s^{-1}$.

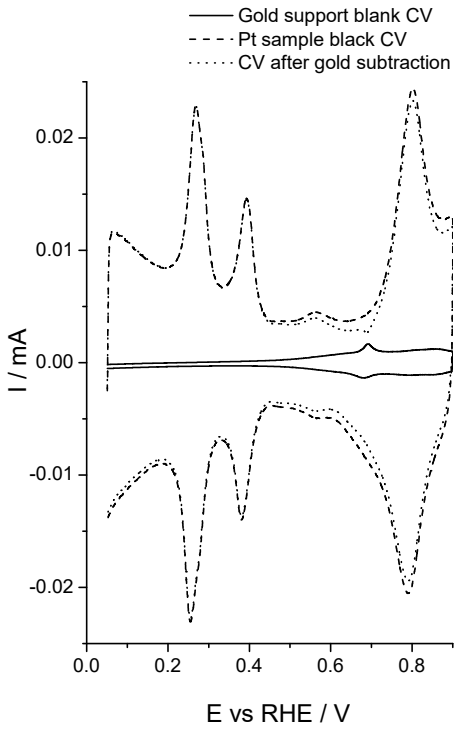


**Figure 5**. Voltammetric profiles of the gold support (solid line), $PtNP_{trunc}$ (dashed line) and $PtNP_{trunc}$ after subtraction of the gold contribution in 0.1 M NaOH. Scan rate 50 mV $s^{-1}$.

In spite of the assumed absence of specific adsorption, the voltammetric profiles also show two main peaks, as in the case of sulfuric acid media, although these peaks appear at higher potentials. The shift towards higher potential values has been already reported for the peaks corresponding to the (110) and (100) steps on the (111) terraces (figure 6).[42] To identify the different adsorption contributions, figure 5 shows the voltammetric response of some Pt single crystal electrodes both basal planes and stepped surfaces, in the same electrolyte. Figure 5A reports the voltammogram of a Pt(111) surface which shows its characteristic OH adsorption contribution on (111) ordered terraces in the potential range between 0.65-0.9 V and a featureless flat signal between 0.06 and 0.3 V. The contributions at high potentials are well-observed in all Pt nanoparticles but its relative intensity strongly depends on their shape. Thus, the $PtNP_{tetra}$ (figure 4C) as well as the $PtNP_{trunc}$ (figure 4D), show a much more intense contribution in agreement with their expected surface structure, since they contain mostly (111) ordered domains.

On the other hand, the (110) contributions both for the basal planes (Pt(110)), and steps (Pt(610) and Pt(775)), can be delimited in the range between 0.15-0.35 V (figure 5C) with a well-marked peak. Remarkably, for (110) terraces (Figure 5C) a clear shoulder is observed; this shoulder is also present in case of the $PtNP_{tetra}$ (figure 4C) and $PtNP_{trunc}$ (figure 4D). The second peak of the voltammograms at ca. 0.4 V contains the contributions from two different types of sites. As in the case of the peak at 0.27 V for sulfuric acid, it contains the contributions from the (100) sites on the (111) terraces as shown for the Pt(755) electrode and also the contributions from the steps on the (100) terraces.[43] As can be seen, this peak is almost absent for the $PtNP_{tetra}$ since the faces of the nanoparticles have a (111) preferential orientation and the presence of (110) steps and defects on these terraces is favorable with respect to the (100) steps. Additionally, the possible rounded edges of the nanoparticles containing (111) faces have a (110) symmetry, which justify the large intensity of the (110) associated peak and the absence of the (100) step related peak.

Regarding the (100) terrace sites, the situation is much more complicated because several adsorption contributions can be observed between 0.2 and 0.65 V for the Pt(100) electrodes.[43-49] However, for a qualitative analysis of the nanoparticles, the characteristic signals coming from (100) terraces can be observed in the potential range between 0.45 and 0.65 V. Interestingly, those Pt nanoparticles with a preferential (100) orientation as in the case of the $PtNP_{cubic}$ (Figure 5B) as well as those containing some smaller (100) terraces as in case of the $PtNP_{trunc}$ (figure 5D), show a broader “double layer” contribution between 0.45 and 0.65 V reflecting the preferential orientation of the samples. This feature contrasts with the case of the preferential (111) nanoparticles ($PtNP_{tetra}$) (figure 5C) which shows a thin “double layer” contribution, in full agreement with the voltammogram obtained with a Pt (111) single crystal electrode. The presence of this (100) characteristic voltammetric feature has very important consequences in the determination of the electroactive surface area in this electrolyte and will be discussed in detail in the following section of this paper.

Regarding the nature of the species giving rise to the different peaks, it should be stressed that most of the signals are due to the competitive adsorption/desorption of H/OH and a clear separation between both processes is not possible. Knowing the adsorbing species on the surface on the

supporting electrolyte can be very important to understand the electrocatalytic activity of the nanoparticles, since the presence of the adsorbed species can catalyze/inhibit the electrochemical process. The measurements of the potential of zero total charge (pztc) can be used to determine the nature of the adsorbed species at the different potentials for surfaces with a well-defined structure. For the Pt(111) electrode, the pztc value lies very close to the so called double layer region (0.33 V) and therefore, the contributions below that potential can be unequivocally assigned to hydrogen adsorption processes whereas the signals between 0.6 and 0.9 V are due to reversible OH adsorption.[42] Unlike this electrode, the potentials of zero total charge measured for the Pt(100) electrode and the stepped surfaces with (111) and (100) terraces lay in regions where significant currents are measured, revealing that currents in these region are due to competitive adsorption desorption of OH/H. For the Pt(100) and stepped surfaces with (100) terraces, the pztc values are 0.44-0.46 V for the surfaces with long terraces and at 0.39-0.40 V for the surfaces with short terraces.[43] In this case, the value matches that of the peak observed in the voltammograms, which clearly indicates that this peak is due to the competitive adsorption desorption of OH/H. A similar situation is found for the stepped surfaces with (111) terraces and (110) monoatomic steps, for which the pztc coincides with that associated to the (110) sites.[50]

Since the adsorption processes on the nanoparticle are determined by the local environment, that is, the local pztc of the site/domain, three different potential regions can be defined. Above 0.6 V, the signal are mainly due to the adsorption of OH on the (111) ordered domains and probably some incipient oxidation/adsorption of OH of the rest of the sites, and for that reason, this region can be unequivocally assigned to OH adsorption. Below 0.2 V, all the signals can be assigned to hydrogen adsorption/desorption processes, since this potential is well below the local pztc of the different sites. The intermediate region (0.2-0.6 V) should be assigned to the competitive adsorption/desorption processes of OH on the surface sites. It should be stressed that this situation is clearly observed in the main peaks.

The results shown up to now clearly indicate that the voltammetric features obtained with different shape-controlled clean Pt nanoparticles (Fig. 4) perfectly correlate with those obtained with Pt single crystal electrodes (Fig. 6). In addition, we have found a good correlation between their characteristic

shapes, estimated by ex-situ TEM measurement, and their preferential surface structures which points out that the indispensable/required manipulation of the samples from the as-prepared colloidal suspension to the "cleaned" water suspension, as well as the final electrochemical cleaning step involving a simple CO adsorption and stripping, does not modify significantly the platinum surface order of the nanoparticles. This fact contrasts with our previous finding in which we evidenced that the UV/ozone irradiation cleaning of shape-controlled Pt nanoparticles, remarkably altered their atomic surface structure, thus significantly modifying their electrocatalytic properties.[51]

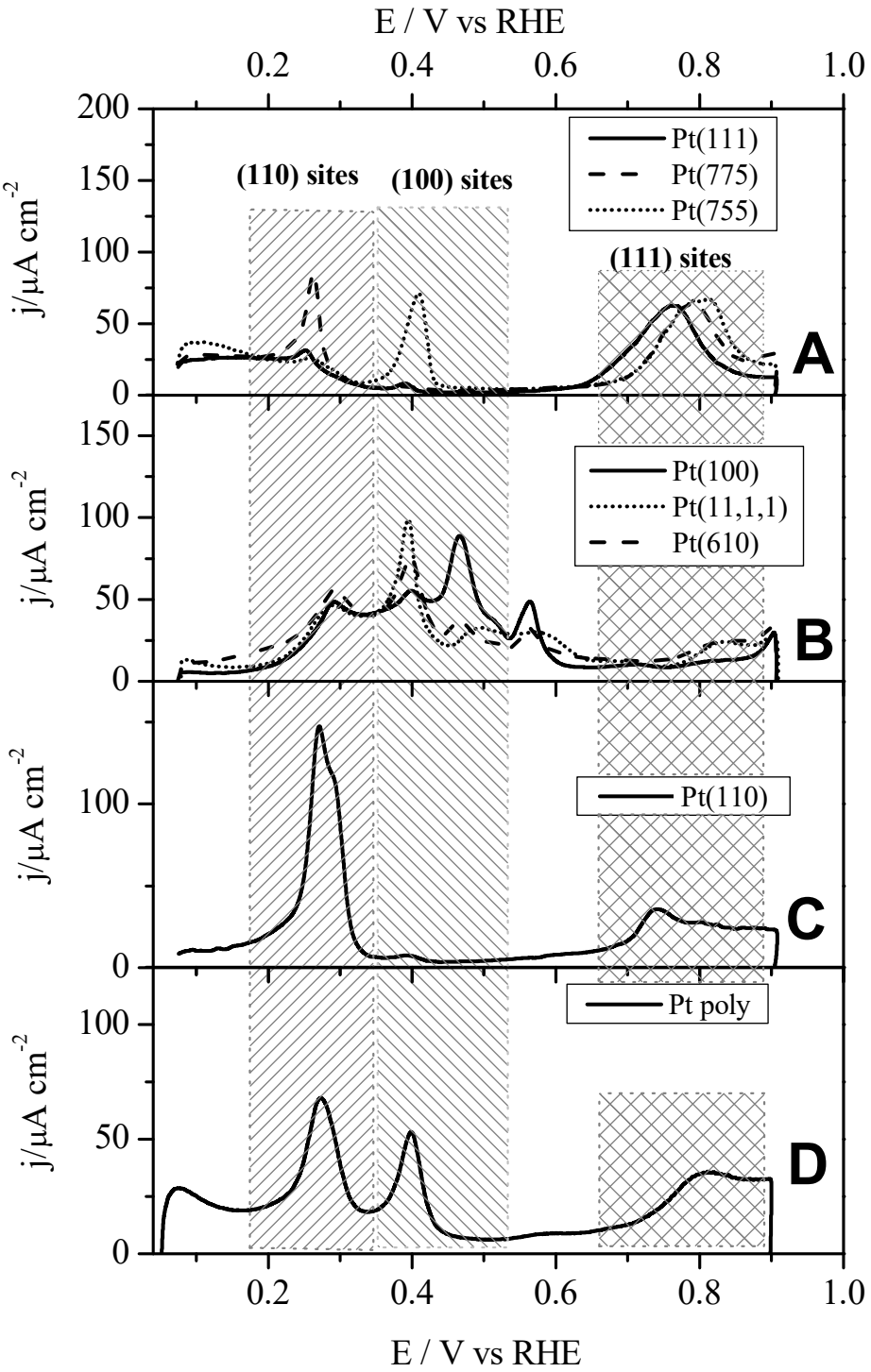


**Figure 6**. Voltammetric profiles of Pt basal planes and different stepped surfaces (A, B and C) and a polyoriented platinum electrode (D) in 0.1 M NaOH. Scan rate: 50 mV $s^{-1}$.

Determination of the electrochemical active surface area in alkaline media

The determination of the active area of electrocatalysts is essential to, first of all, compare the performance of the different electrocatalysts and secondly to prove any enhancement in this

performance. Traditionally, the determination of the active area of platinum has been assessed using the charge measured under the adsorption states at low potentials (the so-called hydrogen adsorption region) for an electrode of known active area. Thus, a reference value for the charge density for this region is obtained and this value can be used to determine the active area of any electrode whose area cannot be measured directly by physical methods. The first reference values for the charge density were obtained for electrochemically cycled polycrystalline samples with no preferential orientation.[52] However, these values could not be appropriate for surfaces with preferential orientations. For instance, surfaces with a large fraction of (111) domains or (100) domains have contributions from these sites at potentials in which the typical polycrystalline platinum has no contributions, as can be seen in figure 1. Recently, the reference values for charge density for platinum electrodes in perchloric and sulfuric acid media have been revisited and reformulated to take into account the possible presence of preferential orientations.[10] As a brief summary, the charge density measured for the region between 0.06 and 0.6 V, after subtraction of the apparent double layer stands for 230 μC $cm^{-2}$ in sulfuric acid solutions whereas in perchloric acid solution the reference value is 200 μC $cm^{-2}$.

For alkaline solutions, the reported reference value is 145 μC $cm^{-2}$ for the charge measured between 0.06 and 0.45 V after the subtraction of the apparent double layer, a significantly lower value than that used in acidic media. In the case of sulfuric or perchloric acid, there is a potential region in which there are no significant contribution from adsorbed species, so that an apparent double layer can be easily determined. Moreover, in the case of sulfuric acid solutions, no contributions are observed between 0.6 and 0.8 V for any single crystal (see figure S4), so that this region can be used to establish the double layer. For alkaline media, there is no such region where significant adsorption processes are absent. For instance, the Pt(111) and stepped surfaces with (111) terraces have a double layer region between 0.45 and 0.6 V. However, large current densities are observed in this region for the surfaces having (100) terrace domains. These distinct contributions can be observed for the different nanoparticles (although at a different extent), so that a clear double layer is not observed. This is especially the case of $PtNP_{cubic}$ for which the apparent double layer

between 0.4 and 0.6 V is larger than in the other cases due to the presence in this region of the adsorption states corresponding to large (100) domains.

In order to determine whether the classical approach was valid for the nanoparticles, the voltammograms for the different samples were recorded initially in sulfuric acid and then immediately transferred to 0.1 M NaOH to record a second voltammogram. The area determined in sulfuric acid is then compared to that estimated in alkaline media by subtracting the apparent double layer measured between 0.45-0.46 V (the potential at which the minimum current is measured) and using a reference value of 145 μC $cm^{-2}$. The determined values from alkaline media are significantly different from those in sulfuric acid, ranging from a -12% difference for the $PtNP_{cubic}$ to an 8% for the $PtNP_{tetra}$.

These differences clearly arise from the selection of the double layer. For the $PtNP_{cubic}$, at 0.45 V the current has a significant contribution from the (100) sites, so that the active area is underestimated. On the other hand, the area is overestimated for the (111) nanoparticles, which have the lowest ratio of (100) sites and lower than the typical polycrystalline sample. These differences mean that the pure double layer contributions cannot be determined in the samples, and a different approach for measuring the active area should be used. For the single crystal electrodes, the total voltammetric charge measured between 0.06 and 0.90 V (without any double layer correction) is very similar for all the electrodes. It should be stressed that in this potential region, the only processes taking place are the hydrogen and OH reversible adsorption. The charges in this region range from 350 μC $cm^{-2}$ for the (111) electrode to 410 μC $cm^{-2}$ for several stepped and kinked surfaces. In fact, the charge values for kinked surfaces have total charge density values between 380 and 400 μC $cm^{-2}$. Due to the small difference in the total charge for the different stepped and kinked surfaces, this value can be used tentatively to calculate the active area in alkaline media. Thus, a reference value for the total charge measured between 0.06 and 0.90 V (without subtraction of double layer) of 390 μC $cm^{-2}$ was chosen and the areas determined using this method compared to those in sulfuric acid. The differences between both measurements are always below ±1.5%, which is below the typical error in this determination. Thus, the new method for measuring the active area in NaOH solutions can be

considered equivalent to that established for sulfuric acid solutions, allowing a direct comparison of the current densities measured in both media. Table 1 summarizes the electroactive surface area results obtained. In addition, for sake of comparison, the surface area estimated from the CO stripping charge in NaOH and using a charge density value of 420 μC $cm^{-2}$, is also included. As it can be observed, the differences between the areas calculated from the CO stripping charges and those previously obtained are now much higher mainly due to the difficulties to establish a baseline correction. In addition, very recently, Chen et al. also concluded that, among various methods, i.e., the adsorption/stripping of adsorbed probe species, such as hydrogen (H), copper (Cu), and carbon monoxide (CO), oxygen and hydroxide (O/ OH), potentiostatic CO/H displacement as well as double layer capacitance to evaluate the electrochemically active surface areas (ECAs) of platinum (Pt) foils, chemically deposited Pt thin film, and carbon-supported Pt nanoparticle electrodes, the CO stripping method was not appropriate for the determination of ECA of rough film nano-Pt with high dispersion, since adsorbed CO molecules caused a significant annealing effect (more than 20% decrease in ECAs after four consecutive times of adsorption and stripping).[53]

| | NaOH /$cm^2$ | $H_2SO_4$ /$cm^{-2}$ | Relative error / % | $CO_{strip}$ in NaOH /$cm^{-2}$ | Relative error / % |
|---|---|---|---|---|---|
| $PtNP_{sphe}$ | 0.726 | 0.717 | +1.3 | 0.677 | -5.5 |
| $PtNP_{cubic}$ | 0.565 | 0.570 | -0.9 | 0.555 | -2.7 |
| $PtNP_{tetra}$ | 0.166 | 0.164 | +1.3 | 0.158 | -3.8 |
| $PtNP_{trunc}$ | 0.385 | 0.380 | +1.1 | 0.332 | -12.7 |
| Poly Pt | 0.195 | 0.193 | +1.0 | 0.205 | +6.4 |

**Table 1**. Comparison of the active surface area values obtained for the different shape-controlled Pt nanoparticles and for a polycrystalline Pt electrode.

CO stripping at shape-controlled Pt nanoparticles in alkaline medium

CO oxidation on platinum electrodes in alkaline media exhibits some characteristics that clearly differentiate its behavior from that observed in acidic solutions. In acidic media, essentially a single stripping peak is observed on the different single crystal surfaces, independently of the symmetry of the terrace or the presence of steps. On the other hand, CO oxidation on stepped and kinked surfaces with (111) terraces in alkaline solution give rise to several peaks, associated to the different sites of the surface. Thus, the CO stripping voltammogram on kinked surfaces with (111) terraces exhibits three different peaks at 0.59, 0.70 and 0.78 V which corresponds to the oxidation of CO on the (110) step (kink) sites, on the (100) step (kink) sites and (111) terrace sites, respectively.[18, 20-22] It has been proposed that the multiple peaks are due to the low mobility of CO on the (111) terraces.[18, 22] On the other hand, only one peak is observed for the stepped surfaces with (100) terraces, which suggests a faster mobility of CO on that type of domain.[43] In this latter case, the presence of steps catalyzes the oxidation of CO, because the peak shifts towards lower potential values as the step density increases. For the stepped surfaces with (100) terraces, the peak appears between 0.62-0.67 V. Additionally, a significant prewave at ca. 0.50 V is observed for all the surfaces, which has been associated to the oxidation of compressed CO adlayers. [18, 22, 54, 55]

This complex dependence of the CO oxidation behavior in alkaline media on the surface structure also affects the behavior of the polycrystalline electrode. As shown in figure 7, the CO stripping voltammogram shows a pre-peak and multiple oxidation peaks, which can be associated to the different surface sites present on the electrode. Aside from the initial prewave, the broad contribution from 0.52 to 0.60 V contains multiple peaks not well resolved, as can be recognized from its irregular shape. These contributions are coming probably from zero and one dimensional domains (defects, steps and kinks), but owing to the heterogeneous nature of the surface, it cannot be easily assigned to the different sites on the surface. When compared to the situation observed in acid solutions, the peak is shifted ca. 100 mV towards lower potentials with respect to that measured in sulfuric acid solutions, a clear indication of the higher activity for CO oxidation of platinum in this medium. Also, the two peaks in sulfuric acid solutions are linked to the short- and long-range

ordered domains of the polycrystalline electrode, as has been determined by the comparison between stepped surfaces and preferentially polyoriented nanoparticles.[28]

When the CO oxidation reaction is studied on the nanoparticles (fig. 8), different behaviors can be observed for the different nanoparticles. Some of them can be directly related to the observed behavior of the single crystal electrodes. The behavior of the $PtNP_{sphe}$ is very similar to that observed for the polycrystalline electrode (figure 7B). A broad contribution between 0.52 and 0.60 V is observed with the main peak at 0.67 V. The major difference is that the charge for the main peak is larger in the case of the nanoparticles, probably related to a slightly different distribution of the sites in the two electrodes. At this respect, the profiles for both hydrogen adsorption in the low potential range and OH adsorption above this electrode potential are slightly different, which probably affects CO oxidation. It should be stressed that for this medium no significant agglomeration effects in the CO stripping peaks have been found. Unlike the observed behavior of the spherical nanoparticles in acid media [56], the CO stripping peak potentials for samples dispersed on carbon in which the nanoparticles are isolated are almost identical to that reported in figure 7.

For the $PtNP_{cubic}$ sample, the expected behavior would be a single peak around 0.62-0.67 V, as observed for the stepped surfaces with narrow (100) terraces. In fact, this peak is observed at 0.67 V, which indicates that the mean size of the ordered domains in relatively small.[43] Additionally, there is peak at 0.60 V that can be assigned to the presence of zero and one order domains as in the case of the polycrystalline electrode.

A completely different case is that of the $PtNP_{tetra}$ and $PtNP_{trunc}$ electrodes. If the behavior of the stepped and kinked surfaces with (111) terraces could be directly extrapolated to the $PtNP_{tetra}$,[18] a significant contribution would be expected at ca. 0.57 V, linked to the presence of (110) defect sites on (111) terraces and other minor contributions at higher potentials, linked to the (100) defects (whose peak at 0.4 V in the blank voltammogram is almost absent) and (111) terraces. The contribution at 0.57 V is present, but the main peak is observed at 0.65 V, which has not been observed for any stepped or kinked surface with (111) terraces. A very similar situation is observed for the $PtNP_{trunc.}$ Thus, this additional peak has to be related either to sites present in the nanoparticles at a significant ratio and absent from stepped and kinked surfaces (edge sites)[57] or to a

modified reactivity of the nanoparticles with (111) domains. In order to study the role of the defects and edge sites on the CO oxidation mechanism, submonolayer coverages of bismuth were deposited on the nanoparticles and CO oxidation was studied on those modified nanoparticles. Bismuth deposition on stepped surfaces with (111) terraces and tetrahedral nanoparticles is a stepwise process nanoparticles, in which the deposition takes place initially on the steps and defect sites and only when these sites have been covered deposition process continues on the terrace.[57, 58] Additionally, Bi on the (111) terrace shows a characteristic redox peak at 0.625 V[59]. Two different Bi coverages on the nanoparticles have been studied (inset figure 9). In the first one, (110) and (100) defects sites have been partially covered but no Bi has been yet deposited on the (111) domains. In the second one, there is already some Bi on the terraces and all the (110) and (100) sites have been covered. The CO stripping voltammograms in alkaline media for those electrodes are shown in figure 9. Several changes can be noticed in the stripping voltammograms as compared to that obtained for the unmodified nanoparticles. First, stripping peaks shift toward positive potentials, in a similar way that is found in acid media.[57] Second, the peak al lower potential completely disappear when all the (110) sites have been covered, confirming the relationship between these peak and the (110) sites. Third, the peak at 0.65 V moves toward positive potential values and becomes wider with the additional appearance of shoulder when (110) and (100) sites have been completely blocked. In this situation, only (111) ordered domains are not blocked on the surface. As has been already proposed, these decorated $PtNP_{tetra}$ electrodes have relatively wide (111) domains and also isolated sites which could adsorb solely hydrogen. Since the only observed CO stripping peak in this situation is that at 0.70 V, which corresponds to that observed at 0.65 V, this peak should be related to the stripping of CO that was initially adsorbed on the (111) ordered domains. The reason why the reactivity of these domains is higher than that observed for the (111) terraces is still not clear. In order to understand such changes in the reactivity, more work is under progress. For the $PtNP_{trunc}$ electrodes, the situation is very similar to that described for the $PtNP_{tetra}$. For this sample, the only difference is that the relative intensities of the different peaks.

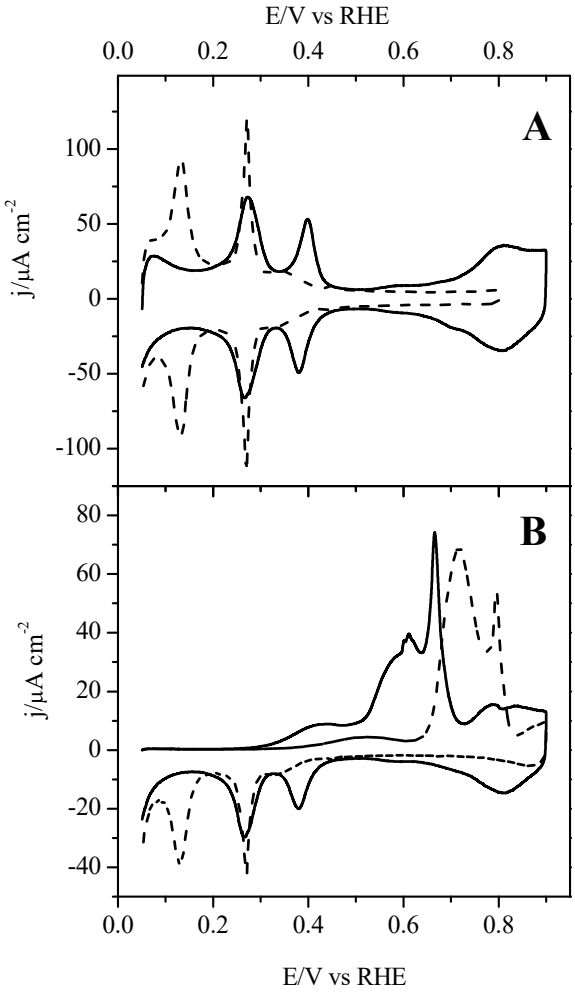


**Figure 7**. A) Voltammetric profiles of a polycrystalline electrode in 0.1 M NaOH (full line) and 0.5 M $H_2SO_4$ (dashed line) (scan rate: 50 mV $s^{-1}$) B) CO stripping voltammograms in 0.1 M NaOH (full line) and 0.5 M $H_2SO_4$ (dashed line) (scan rate: 20 mV $s^{-1}$)

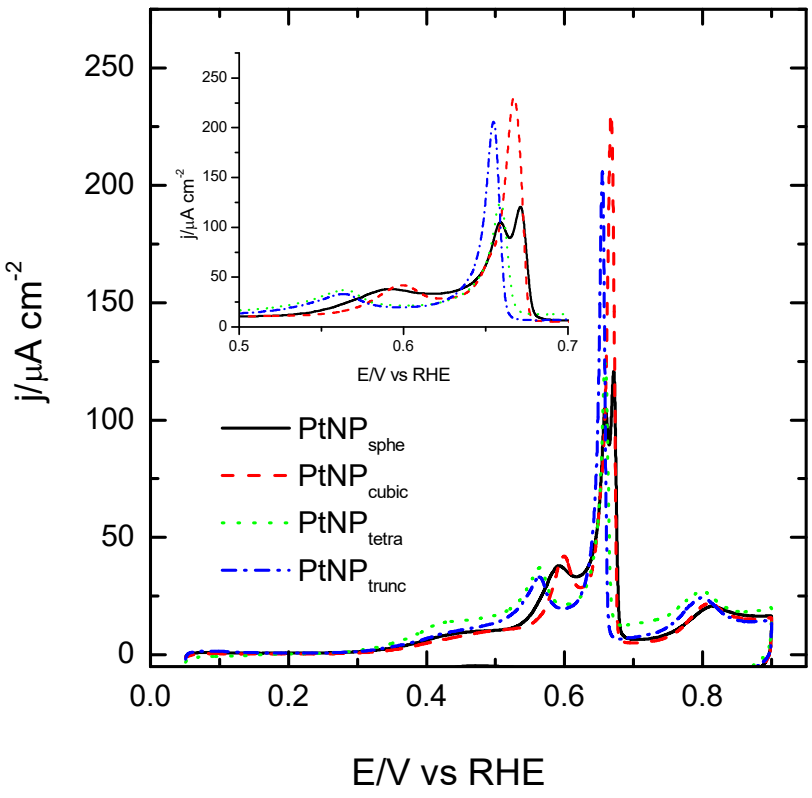


**Figure 8**. CO stripping voltammogram in 0.1 M NaOH for $PtNP_{sphe}$, $PtNP_{cubic}$, $PtNP_{tetra}$ and $PtNP_{trunc}$. Scan rate: 20 mV $s^{-1}$.

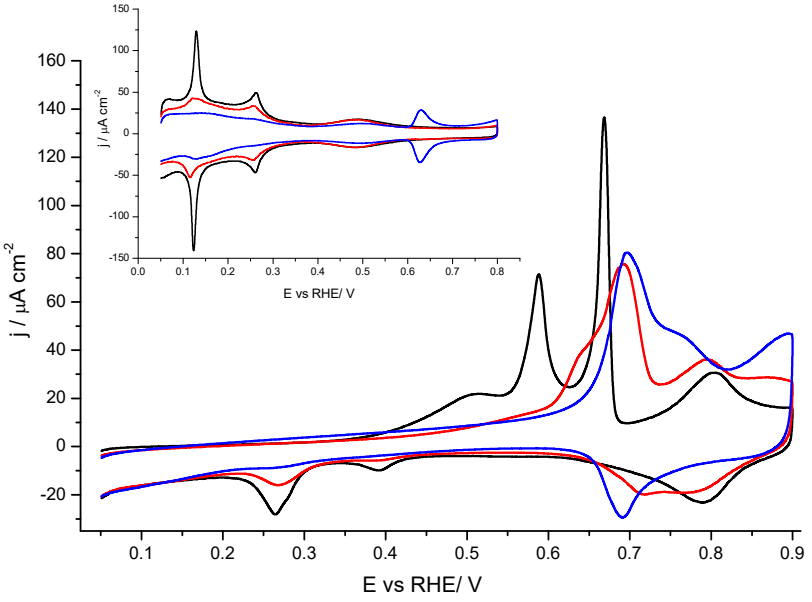


**Figure 9**. CO stripping voltammogram in 0.1 M NaOH for $PtNP_{tetra}$ modified with Bi adatoms. Scan rate: 20 mV $s^{-1}$. Inset: voltammograms corresponding to $PtNP_{tetra}$ modified with Bi adatoms in 0.5 M $H_2SO_4$. Scan rate 50 mV $s^{-1}$.

## Conclusions

The analysis of the results in the different media demonstrates that the voltammetric profile of the platinum nanoparticles in sulfuric acid, perchloric acid and alkaline media can be used as characterization tool of the surface structure of the nanoparticles. Although the surface structure of the nanoparticles is always much more complex than that of the platinum single crystal, a good correlation between the voltammograms and the average shape of the nanoparticles determined by TEM is obtained. The characteristic peaks can be employed to determine whether the nanoparticles have been cleaned from the surfactants used during the synthetic procedures. Additionally, for the nanoparticle characterization and determination of the electrocatalytic activity, it is very important an accurate determination of the active area of the electrocatalysts. For that reason, a new criterion for estimating the active surface area of the nanoparticles in alkaline media has been established. For this media, the total charge measured between 0.06 and 0.90 V (without any double layer correction) stands for 390 $\mu C\ cm^{-2}$. The areas determined with this method are in perfect agreement with those measured in acidic media. For CO oxidation experiments, it has been found that the edge sites play a key role in the behavior of the nanoparticles, since the major peak can be ascribed to the oxidation of CO on these sites.

ACKNOWLEDGMENTS. This work has been financially supported by the MICINN (Spain) (project CTQ2010-16271) and Generalitat Valenciana (project PROMETEO/2009/045, -FEDER).

SUPPORTING INFORMATION PARAGRAPH. The supporting information contains the detailed experimental procedure for the synthesis of the nanoparticles, together with data from the TEM characterization and the quantification of the different surface sites obtained from the irreversible adsorption of Ge and Bi.

REFERENCES


1. Markovic, N. M.; Gasteiger, H. A.; Ross, P. N., *Journal of Physical Chemistry* **1995,** *99* (11), 3411-3415.
2. Maciá, M. D.; Campina, J. M.; Herrero, E.; Feliu, J. M., *Journal of Electroanalytical Chemistry* **2004,** *564* (1-2), 141-150.
3. Kuzume, A.; Herrero, E.; Feliu, J. M., *Journal of Electroanalytical Chemistry* **2007,** *599* (2), 333-343.
4. Koper, M. T. M.; Lai, S. C. S.; Herrero, E., Mechanisms of the Oxidation of Carbon Monoxide and Small Organic Molecules at Metal Electrodes. In *Fuel Cell Catalysis, A Surface Science Approach*, Koper, M. T. M., Ed. John Wiley & Sons, Inc: Hoboken, NJ, 2009; pp 159-208.
5. Vidal-Iglesias, F. J.; Solla-Gullón, J.; Rodríguez, P.; Herrero, E.; Montiel, V.; Feliu, J. M.; Aldaz, A., *Electrochemistry Communications* **2004,** *6* (10), 1080-1084.
6. Solla-Gullon, J.; Vidal-Iglesias, F. J.; Feliu, J. M., *Annual Reports Section "C" (Physical Chemistry)* **2011,** *107* (0), 263-297.
7. Koper, M. T. M., *Nanoscale* **2011,** *3* (5), 2054-2073.
8. Lee, I.; Delbecq, F.; Morales, R.; Albiter, M. A.; Zaera, F., *Nat Mater* **2009,** *8* (2), 132-138.
9. Sanchez-Sanchez, C. M.; Solla-Gullon, J.; Vidal-Iglesias, F. J.; Aldaz, A.; Montiel, V.; Herrero, E., *Journal of the American Chemical Society* **2010,** *132* (16), 5622-5624.
10. Chen, Q. S.; Solla-Gullon, J.; Sun, S. G.; Feliu, J. M., *Electrochim Acta* **2010,** *55* (27), 7982-7994.
11. Clavilier, J., Flame-Annealing and Cleaning Technique. In *Interfacial Electrochemistry*, Wieckowski, A., Ed. Marcel Dekker, Inc.: New York, 1999; pp 231-248.
12. Rodes, A.; Elachi, K.; Zamakhchari, M. A.; Clavilier, J., *Journal of Electroanalytical Chemistry* **1990,** *284* (1), 245-253.
13. Clavilier, J.; Elachi, K.; Rodes, A., *Journal of Electroanalytical Chemistry* **1989,** *272* (1-2), 253-261.
14. Parsons, R.; Ritzoulis, G., *Journal of Electroanalytical Chemistry* **1991,** *318* (1-2), 1-24.
15. Furuya, N.; Koide, S., *Surface Science* **1989,** *220* (1), 18-28.
16. Clavilier, J., *ACS Symposium Series* **1988,** *378*, 202-215.
17. Clavilier, J.; Elachi, K.; Rodes, A., *Chemical Physics* **1990,** *141* (1), 1-14.
18. Herrero, E.; Chen, Q.-S.; Hernandez, J.; Sun, S.-G.; Feliu, J. M., *Physical Chemistry Chemical Physics* **2011,** *13*, 16762-16771.
19. García, G.; Koper, M. T. M., *ChemPhysChem* **2011,** *12* (11), 2064-2072.
20. Garcia, G.; Koper, M. T. M., *Journal of the American Chemical Society* **2009,** *131* (15), 5384-5385.
21. Garcia, G.; Koper, M. T. M., *Physical Chemistry Chemical Physics* **2009,** *11* (48), 11437-11446.
22. Garcia, G.; Koper, M. T. M., *Physical Chemistry Chemical Physics* **2008,** *10* (25), 3802-3811.
23. Solla-Gullón, J.; Montiel, V.; Aldaz, A.; Clavilier, J., *Journal of the Electrochemical Society* **2003,** *150* (2), E104-E109.
24. Solla-Gullón, J.; Rodríguez, P.; Herrero, E.; Aldaz, A.; Feliu, J. M., *Physical Chemistry Chemical Physics* **2008,** *10* (10), 1359-1373.
25. Solla-Gullón, J.; Vidal-Iglesias, F. J.; López-Cudero, A.; Garnier, E.; Feliu, J. M.; Aldaz, A., *Physical Chemistry Chemical Physics* **2008,** *10* (25), 3689-3698.
26. Vidal-Iglesias, F. J.; Solla-Gullon, J.; Perez, J. M.; Aldaz, A., *Electrochemistry Communications* **2006,** *8* (1), 102-106.
27. Ahmadi, T. S.; Wang, Z. L.; Green, T. C.; Henglein, A.; El-Sayed, M. A., *Science* **1996,** *272* (5270), 1924-1926.

28. Solla-Gullón, J.; Vidal-Iglesias, F. J.; Herrero, E.; Feliu, J. M.; Aldaz, A., *Electrochemistry Communications* **2006,** *8* (1), 189-194.
29. Clavilier, J.; Armand, D.; Sun, S. G.; Petit, M., *Journal of Electroanalytical Chemistry* **1986,** *205* (1-2), 267-277.
30. Rodes, A.; Zamakhchari, M. A.; Elachi, K.; Clavilier, J., *Journal of Electroanalytical Chemistry* **1991,** *305* (1), 115-129.
31. Al-Akl, A.; Attard, G.; Price, R.; Timothy, B., *Physical Chemistry Chemical Physics* **2001,** *3* (16), 3261-3268.
32. Rodríguez, P.; Herrero, E.; Solla-Gullón, J.; Vidal-Iglesias, F. J.; Aldaz, A.; Feliu, J. M., *Electrochim Acta* **2005,** *50* (21), 4308-4317.
33. Rodríguez, P.; Solla-Gullón, J.; Vidal-Iglesias, F. J.; Herrero, E.; Aldaz, A.; Feliu, J. M., *Analytical Chemistry* **2005,** *77* (16), 5317-5323.
34. Solla-Gullón, J.; Vidal-Iglesias, F. J.; Rodríguez, P.; Herrero, E.; Feliu, J. M.; Clavilier, J.; Aldaz, A., *Journal of Physical Chemistry B* **2004,** *108* (36), 13573-13575.
35. Rodríguez, P.; Herrero, E.; Solla-Gullón, J.; Vidal-Iglesias, E. J.; Aldaz, A.; Feliu, J. M., *Electrochim Acta* **2005,** *50* (15), 3111-3121.
36. Rodríguez, P.; Herrero, E.; Aldaz, A.; Feliu, J. M., *Langmuir* **2006,** *22* (25), 10329-10337.
37. Gómez, R.; Orts, J. M.; Alvarez-Ruiz, B.; Feliu, J. M., *Journal of Physical Chemistry B* **2004,** *108* (1), 228-238.
38. Climent, V.; Gómez, R.; Orts, J. M.; Feliu, J. M., *Journal of Physical Chemistry B* **2006,** *110* (23), 11344-11351.
39. Kibler, L. A.; Cuesta, A.; Kleinert, M.; Kolb, D. M., *Journal of Electroanalytical Chemistry* **2000,** *484* (1), 73-82.
40. Gómez, R.; Clavilier, J., *Journal of Electroanalytical Chemistry* **1993,** *354* (1+2), 189-208.
41. Souza-Garcia, J.; Climent, V.; Feliu, J. M., *Electrochemistry Communications* **2009,** *11* (7), 1515-1518.
42. Climent, V.; Gómez, R.; Orts, J. M.; Aldaz, A.; Feliu, J. M., Potential of Zero Total Charge of Platinum Single Crystal Electrodes. The Electrochemical Society, Inc.: Pennington, NJ, 2000; Vol. 2000-16, pp 12-30.
43. Arán-Ais, R. M.; Figueiredo, M. C.; Vidal-Iglesias, F. J.; Climent, V.; Herrero, E.; Feliu, J. M., *Electrochim Acta* **2011,** *58* (0), 184-192.
44. Vidal-Iglesias, F. J.; Solla-Gullón, J.; Montiel, V.; Feliu, J. M.; Aldaz, A., *Journal of Physical Chemistry B* **2005,** *109* (26), 12914-12919.
45. Vidal-Iglesias, F. J.; Garcia-Araez, N.; Montiel, V.; Feliu, J. M.; Aldaz, A., *Electrochemistry Communications* **2003,** *5* (1), 22-26.
46. Schmidt, T. J.; Ross, P. N.; Markovic, N. M., *Journal of Physical Chemistry B* **2001,** *105* (48), 12082-12086.
47. Markovic, N. M.; Gasteiger, H. A.; Philip, N., *Journal of Physical Chemistry B* **1996,** *100* (16), 6715-6721.
48. Rodes, A.; Climent, V.; Orts, J. M.; Pérez, J. M.; Aldaz, A., *Electrochim Acta* **1998,** *44* (6-7), 1077-1090.
49. van der Vliet, D. F.; Koper, M. T. M., *Surface Science* **2010,** *604* (21-22), 1912-1918.
50. Unpublished results
51. Vidal-Iglesias, F. J.; Solla-Gullón, J.; Herrero, E.; Montiel, V.; Aldaz, A.; Feliu, J. M., *Electrochemistry Communications* **2011,** *13* (5), 502-505.
52. Trasatti, S.; Petrii, O. A., *Pure and Applied Chemistry* **1991,** *63*, 711-734.
53. Chen, D.; Tao, Q.; Liao, L. W.; Liu, S. X.; Chen, Y. X.; Ye, S., *Electrocatalysis* **2011,** *2*, 207-219.
54. Markovic, N. M.; Ross, P. N., *Surface Science Reports* **2002,** *45* (4-6), 121-229.
55. Spendelow, J. S.; Goodpaster, J. D.; Kenis, P. J. A.; Wieckowski, A., *Journal of Physical Chemistry B* **2006,** *110* (19), 9545-9555.
56. López-Cudero, A.; Solla-Gullón, J.; Herrero, E.; Aldaz, A.; Feliu, J. M., *Journal of Electroanalytical Chemistry* **2010,** *644* (2), 117-126.
57. Chen, Q. S.; Vidal-Iglesias, F. J.; Solla-Gullón, J.; Sun, S. G.; Feliu, J. M., *Chemical Science* **2012,** *3* (1), 136-147.

58. Herrero, E.; Climent, V.; Feliu, J. M., *Electrochemistry Communications* **2000,** *2* (9), 636-640.
59. Clavilier, J.; Feliu, J. M.; Aldaz, A., *Journal of Electroanalytical Chemistry* **1988,** *243* (2), 419-433.

GRAPHICAL ABSTRACT

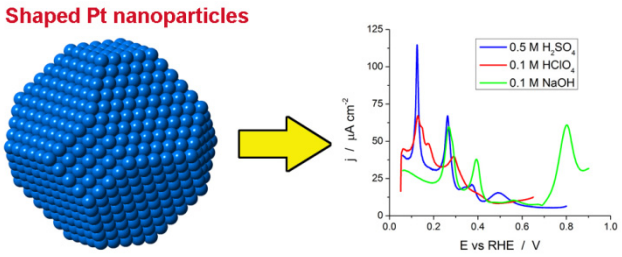

# Electrochemical characterization of shape-controlled Pt nanoparticles in different supporting electrolytes

*Francisco J. Vidal-Iglesias, Rosa M. Arán-Ais, José Solla-Gullón, Enrique Herrero*, Juan M. Feliu*

Instituto de Electroquímica, Universidad de Alicante, Apartado 99, 03080 Alicante (Spain)

## SUPPORTING INFORMATION

**Synthesis and cleaning of the Pt nanoparticles**

In this work four types of Pt nanoparticles were prepared.

i) Pt nanoparticles with preferential **spherical shape** ($PtNP_{sphe}$) were synthesized by reducing $H_2PtCl_6$ with sodium borohydride using a water-in-oil (w/o) microemulsion of water (3%) /polyethylene glycol dodecyl ether (BRIJ®30) (16.5%) / n-heptane (80.5%) in a similar methodology to that previously reported.[1-3] The values in brackets represent the volume percentage of each compound. The synthesis was performed by directly adding $NaBH_4$ to the micellar solution. The concentration of the $H_2PtCl_6$ in the water phase was 0.1 M and the concentration of the added sodium borohydride was 1 M. After complete reduction, which takes place in a few minutes, acetone was added to the solution to cause phase separation. Afterwards, these Pt NPs were cleaned with successive acetone, acetone-water mixtures and water washes to finally achieve a water suspension with clean spherical nanoparticles. This procedure allows cleaning the nanoparticles avoiding electrochemical adsorption of oxygen and thus preserving the initial surface structure of the nanoparticles. Finally the nanoparticles were stored in ultra-pure water as a suspension.

ii) Pt nanoparticles with preferential **cubic shape** ($PtNP_{cubic}$) were synthesized with a colloidal method using sodium polyacrylate (PA, Mw = 2100) as a capping agent and $K_2PtCl_4$ as a metallic precursor ($10^{-4}$ M aqueous aged solution).[3-5] The ratio of $K_2PtCl_4$ to PA was (1:5). Then, this colloidal suspension was purged with Ar gas for 20 min and finally bubbled with $H_2$ gas for 5 min to reduce the Pt precursor. The reaction vessel was then sealed and the solution was left overnight.

iii) Pt nanoparticles with preferential **octahedral and tetrahedral shape** ($PtNP_{tetra}$) were synthesized by a colloidal method using PA as a capping agent and $H_2PtCl_6$ as a metallic precursor ($10^{-4}$ M aqueous aged solution). [3-5] The ratio of $H_2PtCl_6$ to PA was (1:5). The suspension pH was adjusted to 7 with 0.1 M HCl solution. Then, this colloidal suspension was

purged with Ar gas for 5 min and finally bubbled with $H_2$ gas for 1 min to reduce the Pt precursor. The reaction vessel was then sealed and the solution was left overnight.

iv) Pt nanoparticles with preferential **truncated octahedral and tetrahedral** ($PtNP_{trunc}$) shape were synthesized by a colloidal method using PA as a capping agent and $H_2PtCl_6$ as a metallic precursor ($10^{-4}$ M aqueous aged solution). [3-5] The ratio of $H_2PtCl_6$ to PA was (1:5). The suspension pH was adjusted to 7 with 0.1 M HCl solution. Then, this colloidal suspension was purged with Ar gas for 10 min and finally bubbled with $H_2$ gas for 5 min to reduce the Pt precursor. The reaction vessel was then sealed and the solution was left overnight.

**Table 1.** Crystallographic description of the platinum single crystal electrodes used in this work

| zone | Miller indices | Terrace-step notation |
|---|---|---|
| [01$\bar{1}$] | Pt(11,1,1) | 6(100) x (111) |
| | Pt(755) | 6(111) x (100) |
| | Pt(544) | 9(111) x (100) |
| [1$\bar{1}$0] | Pt(554) | 10(111) x (110) |
| | Pt(775) | 7(111) x (110) |
| [001] | Pt(610) | 6(100)x(110) |

**Table 2.** Percentage of (111) and (100) terrace sites on the different samples measured with bismuth[2, 6, 7] and germanium[2, 8, 9] adsorption procedures

| | (111) sites / % | (100) sites / % |
|---|---|---|
| $PtNP_{sphe}$ | 6 | 14 |
| $PtNP_{cubic}$ | 11 | 52 |
| $PtNP_{tetra}$ | 42 | 3 |
| $PtNP_{trunc}$ | 33 | 17 |

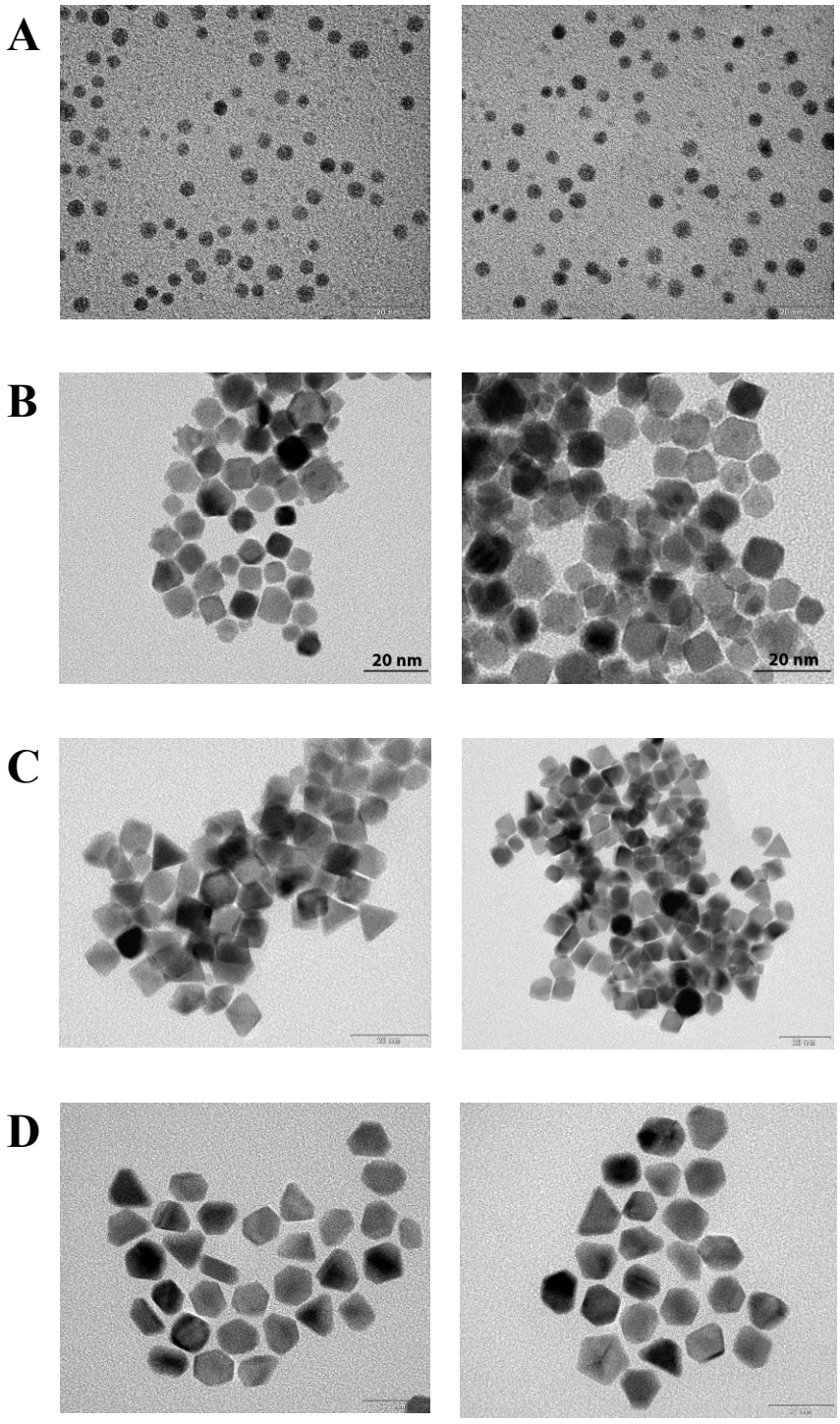


**Figure S1.** Representative TEM images of the (A) $PtNP_{sphe}$, (B) $PtNP_{cubic}$, (C) $PtNP_{tetra}$ and (D) $PtNP_{trunc}$ used in the present paper.

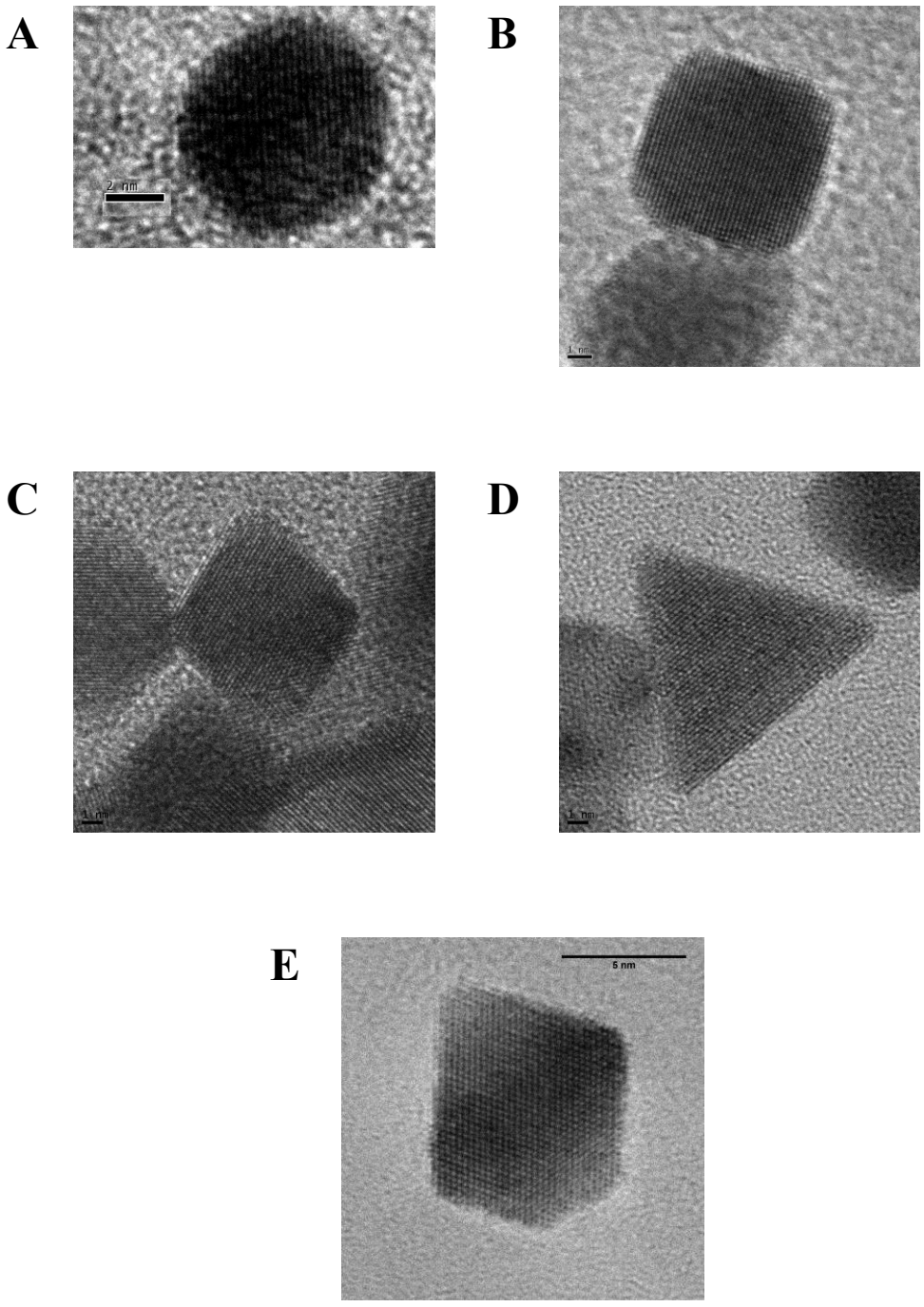


**Figure S2.** Representative HRTEM images of the (A) $PtNP_{sphe}$, (B) $PtNP_{cubic}$, (C) and (D) $PtNP_{tetra}$ and (E) $PtNP_{trunc}$ used in the present paper.

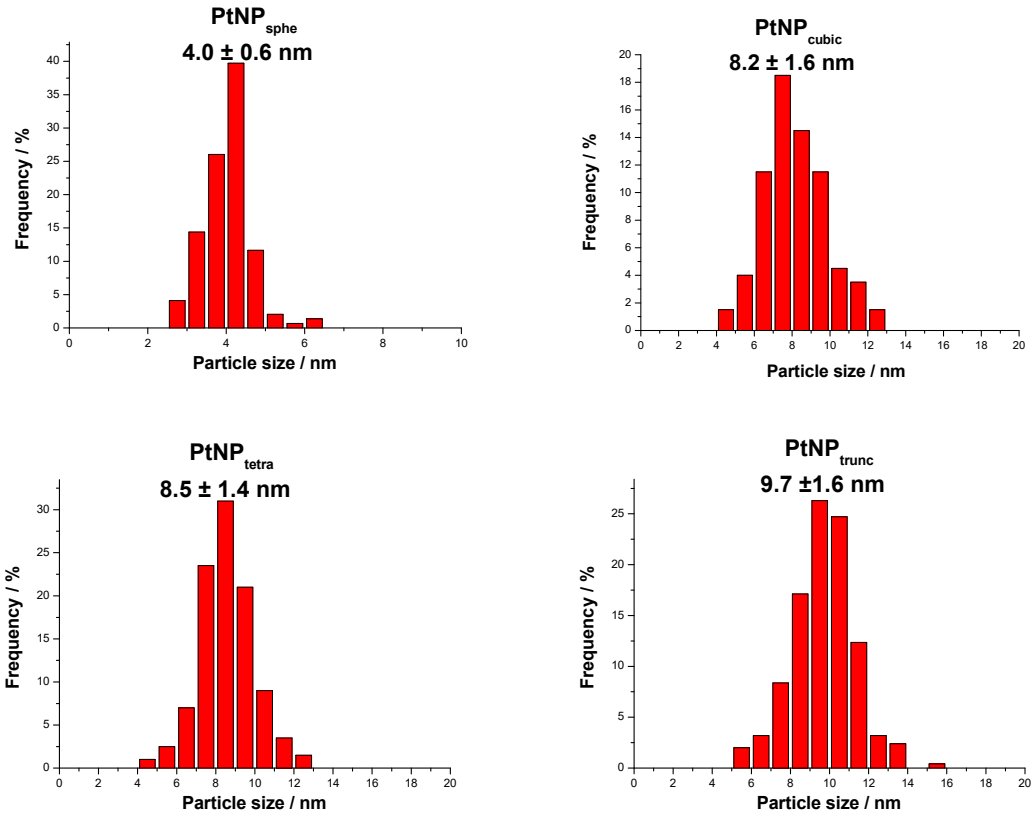


**Figure S3.** Particle size histograms of the different shape controlled Pt nanoparticles used in the present paper.

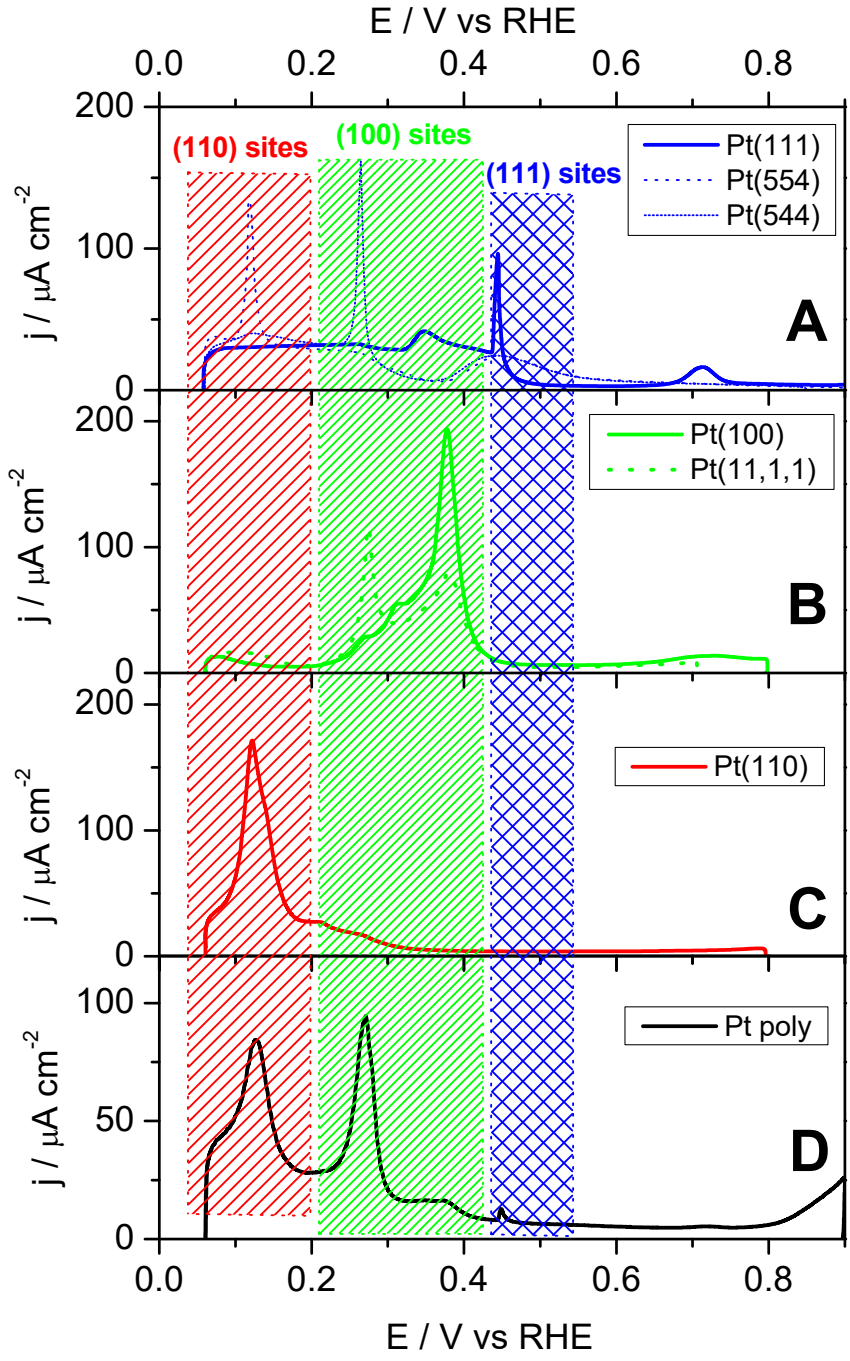


***Figure S4***. Voltammetric profiles of Pt basal planes and different stepped surfaces (A, B and C) and a polyoriented platinum electrode (D). Test solution 0.5 M $H_2SO_4$. Scan rate: 50 mV $s^{-1}$.

## References


1. Solla-Gullón, J.; Montiel, V.; Aldaz, A.; Clavilier, J., *J. Electrochem. Soc.* **2003,** *150* (2), E104-E109.
2. Solla-Gullón, J.; Rodríguez, P.; Herrero, E.; Aldaz, A.; Feliu, J. M., *Phys. Chem. Chem. Phys.* **2008,** *10* (10), 1359-1373.
3. Solla-Gullón, J.; Vidal-Iglesias, F. J.; López-Cudero, A.; Garnier, E.; Feliu, J. M.; Aldaz, A., *Phys. Chem. Chem. Phys.* **2008,** *10* (25), 3689-3698.
4. Ahmadi, T. S.; Wang, Z. L.; Green, T. C.; Henglein, A.; El-Sayed, M. A., *Science* **1996,** *272* (5270), 1924-1926.
5. Solla-Gullón, J.; Vidal-Iglesias, F. J.; Herrero, E.; Feliu, J. M.; Aldaz, A., *Electrochem. Commun.* **2006,** *8* (1), 189-194.
6. Rodríguez, P.; Herrero, E.; Solla-Gullón, J.; Vidal-Iglesias, F. J.; Aldaz, A.; Feliu, J. M., *Electrochim. Acta* **2005,** *50* (21), 4308-4317.
7. Rodríguez, P.; Solla-Gullón, J.; Vidal-Iglesias, F. J.; Herrero, E.; Aldaz, A.; Feliu, J. M., *Anal. Chem.* **2005,** *77* (16), 5317-5323.
8. Solla-Gullón, J.; Vidal-Iglesias, F. J.; Rodríguez, P.; Herrero, E.; Feliu, J. M.; Clavilier, J.; Aldaz, A., *J. Phys. Chem. B* **2004,** *108* (36), 13573-13575.
9. Rodríguez, P.; Herrero, E.; Solla-Gullón, J.; Vidal-Iglesias, E. J.; Aldaz, A.; Feliu, J. M., *Electrochim. Acta* **2005,** *50* (15), 3111-3121.